Novel EMIC Wave Propagation Pathway Through Buchsbaum Resonance and Inter-Hemispheric Wave Interference: Swarm Observations and Modelling

I. P. Pakhotin[1, 2], I.R. Mann[1], D. Sydorenko[1], R. Rankin[1]

[1] Department of Physics, University of Alberta, Edmonton, Alberta, Canada

[2] Department of Physics and Astronomy, University of Calgary, Calgary, Alberta, Canada

Contents of this file

Text S1
Figures S1 to S5
Captions for Movies S1 and S2

Additional Supporting Information (Files uploaded separately)

Movies S1 and S2

Introduction

This Supporting Information contains further material in support of the conclusions of our paper. We provide additional details and description of the simulation model used in the publication, and present movies showing the evolution of the wave energy over time, both in the transverse and compressional B-field components, after the model is initialized with the assumed plasma parameters detailed in the publication. In relation to the Swarm data analysis, it contains figures which further develop on the phase differencing analysis applied to the compressional magnetic field in the Swarm data utilized in the publication to assess the location of the inferred source regions for the waves. It further shows data from Van Allen Probe B

and the CARISMA ground magnetometer array (www.carisma.ca) which augment the Swarm A and C observations.

Text S1.

Equations solved by the numerical model

The model uses spherical coordinates and resolves variations along r and ϑ. Periodicity in the azimuthal direction is assumed with all non-stationary values proportional to $\exp(im\varphi)$, where m is an integer azimuthal wavenumber. The simulation domain is a sector in the meridional plane with $\vartheta_{min} < \vartheta < \vartheta_{max}$ and $R_E < r < r_{max}$, where R_E is the Earth radius and r_{max} is the radius of the outer boundary. It is assumed that azimuthal variations of wave perturbations are described as $\exp(im\varphi)$ where integer m is the azimuthal wavenumber. The model uses dipole geomagnetic field. The ions (H^+, He^+, N^+, O^+, NO^+, and O_2^+) and electrons are represented as fluids. Collisions with neutrals (H, He, N, O, N_2, NO, O_2) are accounted for all charged species. Initial densities and temperatures of electrons, ions, and neutrals are obtained using IRI, GCPM, and MSIS models. The model solves Maxwell equations

$$\frac{\partial \vec{B}}{\partial t} = -\nabla \times \vec{E} \,, \frac{1}{c^2}\frac{\partial \vec{E}}{\partial t} = \nabla \times \vec{B} - \mu_0 \vec{J} \,.$$

The simulation domain includes the air gap between the Earth surface and the bottom of ionosphere, $R_E < r < R_{ion}$, where R_{ion} is the radius of the bottom of the ionosphere. In this gap, the plasma density and the electric current in Ampere's law are zero. In the ionosphere and magnetosphere, the electric current is

$$\vec{J} = \vec{J}_i + \vec{J}_{e,\perp} + \vec{J}_{e,\parallel} + \vec{J}_{ext}$$

where $\vec{J}_i = e \sum_s n_s \vec{u}_s$ is the electric current due to ions, n_s and $\vec{u}_s$ are the density and velocity of ion species s, $\vec{J}_{e,\perp}$ and $\vec{J}_{e,\parallel}$ are the electric currents due to electrons perpendicular and parallel to the geomagnetic field, respectively, $\vec{J}_{ext}$ is the external current driving the wave.

The ion flow velocity is obtained from the linear motion equation

$$\frac{\partial \vec{u}_s}{\partial t} = \frac{e}{m_s}\left(\vec{E} + \vec{u}_s \times \vec{B}_0\right) - \nu_s \vec{u}_s$$

where $\vec{B}_0$ is the geomagnetic field, ν_s is the frequency of collisions with neutrals. The transverse electron current is due to Pedersen and Hall drifts and is calculated as

$$\vec{J}_{e,\perp} = \bar{\bar{R}}\bar{\bar{\sigma}}_{e,\perp}\bar{\bar{R}}^T \vec{E}, \, \bar{\bar{\sigma}}_{e,\perp} = \begin{pmatrix} \sigma_{P,e} & -\sigma_{H,e} & 0 \\ \sigma_{H,e} & \sigma_{P,e} & 0 \\ 0 & 0 & 0 \end{pmatrix}, \bar{\bar{R}} = \begin{pmatrix} 0 & b_\vartheta & b_r \\ 0 & -b_r & b_\vartheta \\ 1 & 0 & 0 \end{pmatrix},$$

where $\sigma_{P,e}$ and $\sigma_{H,e}$ are the electron Pedersen and Hall conductivities, respectively, defined below, b_r and b_ϑ are the components of a unitary vector $\vec{b}$ directed along the dipole geomagnetic field. Matrix $\bar{\bar{R}}^T$ transforms a vector in the spherical coordinate system $\{\hat{r}, \hat{\vartheta}, \hat{\varphi}\}$ into a coordinate system with basis vectors $\{\hat{x}_1, \hat{x}_2, \hat{x}_3\}$ where $\hat{x}_3 = \vec{b}$, $\hat{x}_2 = \vec{b} \times \hat{\varphi}/|\vec{b} \times \hat{\varphi}|$, $\hat{x}_1 = \hat{x}_2 \times \hat{x}_3$. Matrix $\bar{\bar{R}}$ performs the inverse transformation. The parallel electron current $\vec{J}_{e,\parallel} = -en_e\vec{u}_{e,\parallel}$ is calculated with the parallel electron velocity defined by the linear dynamics equation

$$\frac{\partial \vec{u}_{e,\parallel}}{\partial t} = -\frac{e}{m_e}\vec{b}(\vec{b} \cdot \vec{E}) - \nu_e\vec{u}_{e,\parallel},$$

where n_e is the electron density and ν_e is the frequency of electron collisions with neutrals.

In the very bottom of the ionosphere, where the collision frequencies are the largest, the electric current is calculated using the conductivity tensor

$$\vec{J} = \bar{\bar{R}}\bar{\bar{\sigma}}\bar{\bar{R}}^T\vec{E}, \quad \bar{\bar{\sigma}} = \begin{pmatrix} \sigma_P & -\sigma_H & 0 \\ \sigma_H & \sigma_P & 0 \\ 0 & 0 & \sigma_\parallel \end{pmatrix},$$

where $\sigma_P = \sigma_{P,e} + \sum_s \sigma_{P,s}$ is the total Pedersen conductivity, $\sigma_H = \sigma_{H,e} + \sum_s \sigma_{H,s}$ is the total Hall conductivity, $\sigma_\parallel = \sigma_{\parallel,e} + \sum_s \sigma_{\parallel,s}$ is the total conductivity in the parallel direction. For a charged species α (electrons or ions) $\sigma_{P,\alpha} = \frac{n_\alpha q_\alpha}{B_0}\frac{\omega_{c,\alpha}\nu_\alpha}{\nu_\alpha^2 + \omega_{c,\alpha}^2}$, $\sigma_{H,\alpha} = -\frac{n_\alpha q_\alpha}{B_0}\frac{\omega_{c,\alpha}^2}{\nu_\alpha^2 + \omega_{c,\alpha}^2}$, $\sigma_{\parallel,\alpha} = \frac{n_\alpha q_\alpha}{B_0}\frac{\omega_{c,\alpha}}{\nu_\alpha}$, $\omega_{c,\alpha} = \frac{q_\alpha B_0}{m_\alpha}$, $q_\alpha = -e$ for electrons (subscript $\alpha = e$) and $q_\alpha = e$ for ions (subscript $\alpha = s$).

The boundary conditions are $E_{\vartheta,\varphi}(R_E) = 0$, $B_{r,\varphi}(\vartheta_{min,max}, r < R_{ion}) = 0$, $\vec{B}(\vartheta_{min,max}, r \geq R_{ion}) = 0$, $\vec{B}(r_{max}) = 0$.
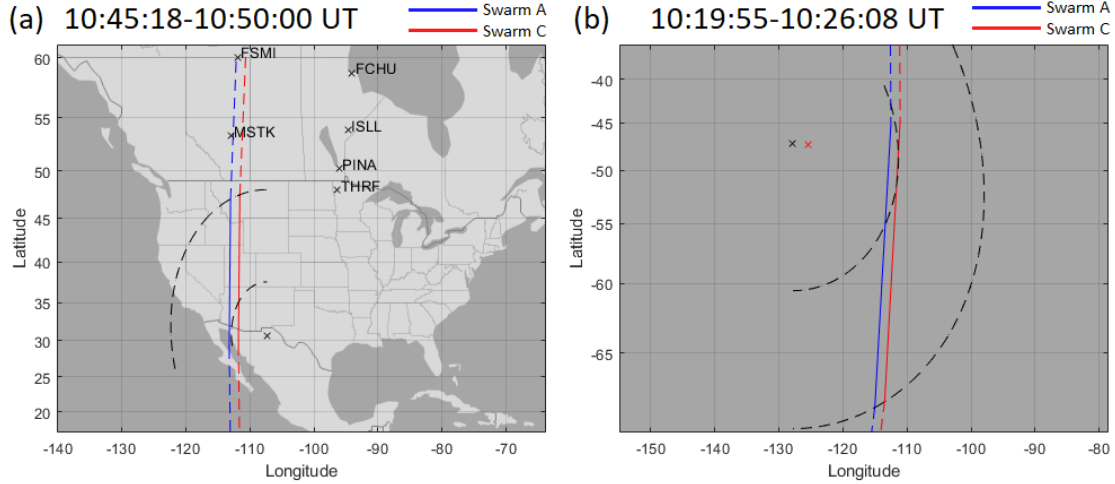
Figure S1. Signal source inference using the phase differencing methodology, as in Figure 1, but without assuming circular propagation of wave fronts. Assuming the Alfven speed does not strongly vary azimuthally between ~5-10 degrees of longitude in this MLT sector, the eccentricity of the ellipse is determined by the ratio of the Alfven speed observed by Swarm A at the point of maximum Swarm A/C phase difference, and the average Alfven speed observed by Swarm A between the point of maximum Swarm A/C phase difference and zero Swarm A/C phase difference. This is applied for both the northern (a) and southern (b) hemispheres. In both cases the ratio is ~0.63. The Alfven speed is estimated using observed magnetic fields, electron density locally from the Langmuir probe on Swarm A assuming a pure O+ plasma. The estimated propagation wave fronts in the areas of interest are plotted as dashed black curves. The ellipse is placed such that its tangent at the point of intersection with Swarm A/C is normal to the Swarm A/C inter-spacecraft separation vector at the point of max phase, and normal to the separation vector at the point of zero phase. The estimated source location is denoted by a black cross; the magnetically conjugate point from the northern hemisphere to the southern hemisphere is denoted by a red cross. A full analysis would require detailed ray tracing, and this is considered to be beyond the scope of this letter.
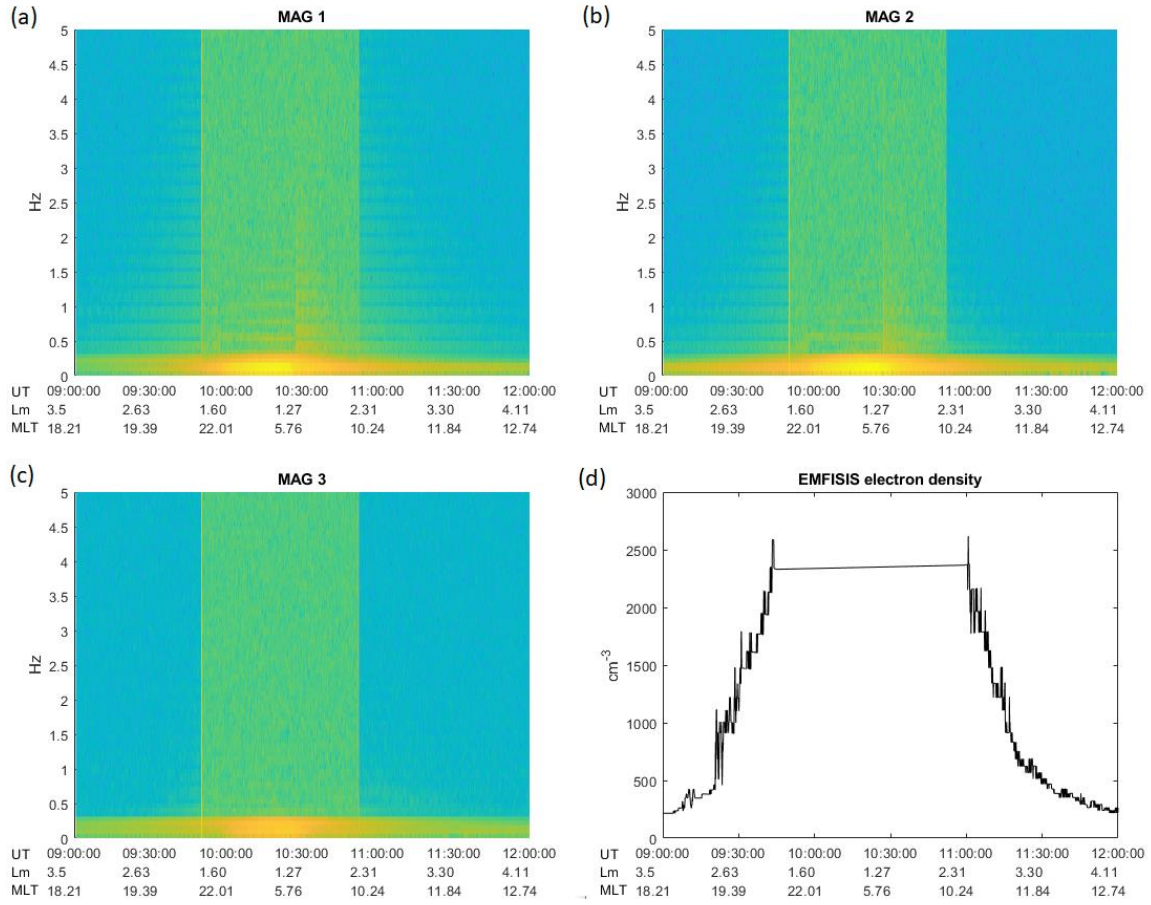
Figure S2. Van Allen Probe B magnetic field dynamic power spectra, with the B-field in MAG coordinates MAG_1 (a), MAG_2 (b) and MAG_3 (c), as well as EMFISIS electron density data (d). The strong emission lines around 0.1 Hz in (a-c) are an artefact of spacecraft spin. No significant EMIC wave activity is detected around 1.5 Hz.
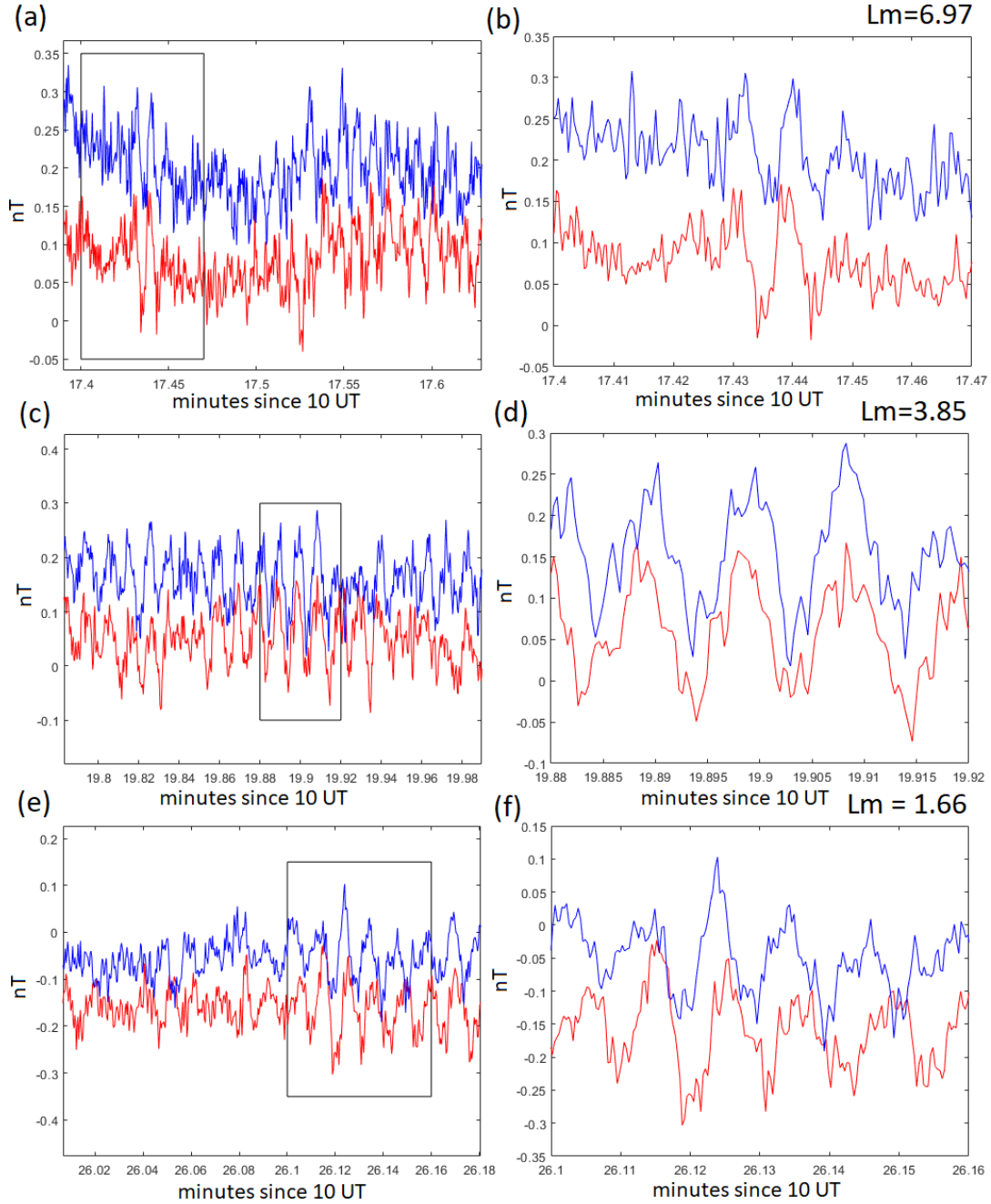
Figure S3. Magnetic field modulus |B| readings for three time periods on Swarm A (blue) and Swarm C (red) as they traversed the southern hemisphere (similar to Figure 3 for the northern hemisphere), the two time series being offset by 0.1 nT for easier viewing. The right column focuses on the areas denoted in the black squares in the left column. In particular, panels (a) and (b) show the period when the wave arrived at the leading Swarm C before Swarm A, panels (c) and (d) show the zero-

phase period, while (e) and (f) show the period where the wave first arrives at the westwards Swarm A and the phase difference is maximum at that point.
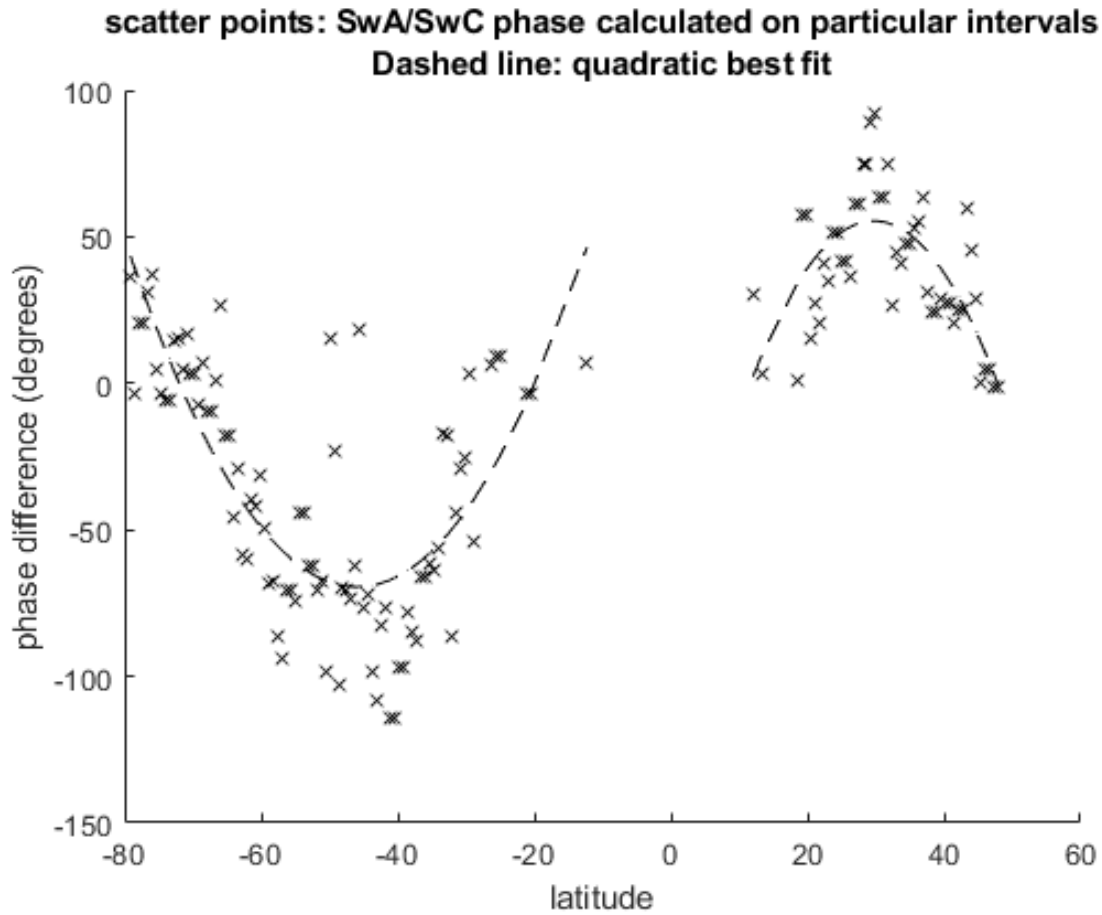

Figure S4. Scatter plot of phase difference between Swarm A and C compressional magnetic field perturbations over a sliding window, as a function of geographic latitude. The dashed lines represent quadratic fits. The plot shows the consistency of the observations with a local source, and with no phase wrap in phase difference between the two spacecraft along their trajectories.
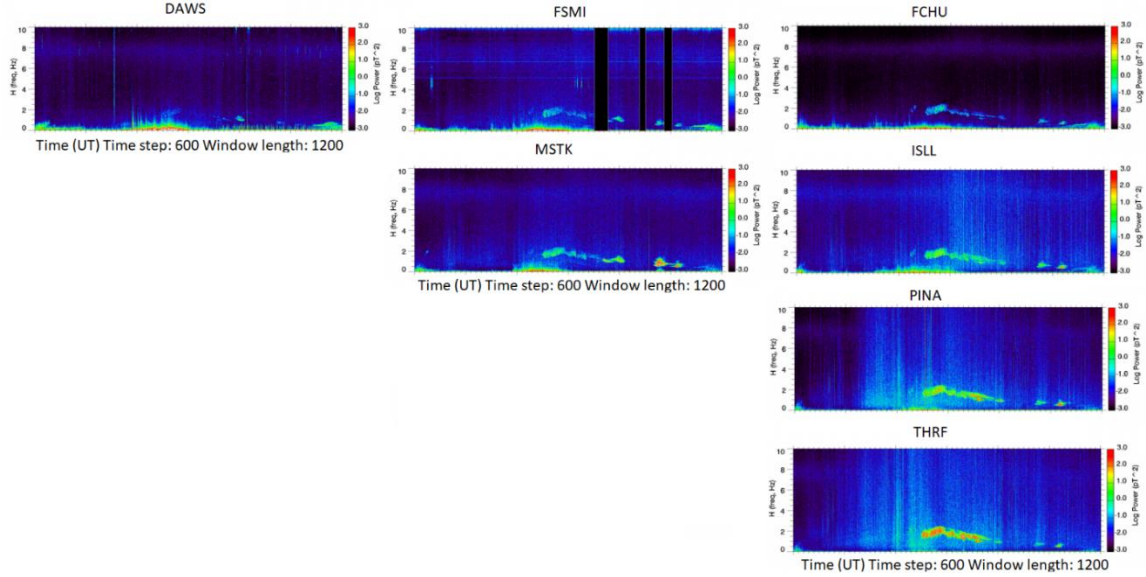
Figure S5. Wave power (H-component) observed at various CARISMA ICM ground stations. The panels are deliberately arranged to reflect the relative geographic position (in latitude and longitude) of the ground stations: lower-latitude ground stations are near the bottom; westwards ground stations are further to the left. It can be seen that wave power is stronger at lower latitudes.

Movie S1. This video shows high-resolution simulation run showing the evolution of the azimuthal magnetic field perturbation in space and time, with the source located in the equatorial plane at 20 x 10^3 km geocentric distance.

Movie S2. This video shows high-resolution simulation run showing the evolution of the δ|B| in space and time, assuming the source is located in the equatorial plane at 20 x 10^3 km geocentric distance.